Observation of surface dissociation of low-energy polyatomic ions relevant to plasma processing

H. Sugai,[a] Y. Mitsuoka, and H. Toyoda
Department of Electrical Engineering, Nagoya University, Chikusa-ku, Nagoya 464-01, Japan

(Received 15 April 1997; accepted 11 August 1997)

To gain insight into surface processes in plasma processing, basic ion beam experiments are performed on two representative polyatomic-ion species: hydrocarbon ions CH_x^+ for deposition processes and fluorocarbon ions CF_x^+ for etching processes ($x=1,2,\ldots$). A single ion species is extracted from an inductive plasma via a mass filter and directed onto aluminum surfaces at energies <150 eV. Significant charge neutralization is observed which leads to backscattering of $\sim 0.3\%$ CH_x^+ ions and $\sim 1\%$ CF_x^+ ions from the surface bombarded at 100 eV. Most of the ions scattered from the surface have kinetic energies lower than 10 eV. A polyatomic ion impinging on the surface breaks up into smaller ionic fragments. Such surface dissociation is found even at very low incident energies (10–50 eV) in the case of hydrocarbon ions, which is attributed to vibrational excitation of the incident parent ions. In contrast to this, fluorocarbon ions hardly dissociate at such low energies. On the other hand, at high energy ($>$ 100 eV) incidence of both CH_x^+ and CF_x^+ species gives rise to dissociation into smaller fragment ions, probably via electronic excitation. © *1998 American Vacuum Society.* [S0734-2101(98)00401-1]

I. INTRODUCTION

There has been a great need to understand ion-surface interactions in plasma-assisted deposition and etching. For example, high-energy surface bombardment by hydrocarbon ions (CH_x^+) from a methane plasma is required to form hard *a*-C:H films with diamondlike properties.[1,2] Space-resolved optical emission studies have recently revealed that energetic ion bombardment yields radicals on solid surfaces by two mechanisms: (i) dissociation of hydrocarbon ions at their impact on the surface and (ii) sputtering of the already deposited *a*-C:H film.[3,4] The threshold energies for yielding the excited CH radical were found to be ~ 20 eV for dissociation and ~ 80 eV for sputtering,[4] along with a dependence on surface materials.[5,6] On the other hand, dry etching of silicon-based materials is currently being performed using fluorocarbon plasmas of such gases as CF_4 and C_4F_8. A recent trend toward high-aspect-ratio damage-free etching requires a deeper understanding of surface processes. As is well known, bombardment of fluorocarbon ions (CF_x^+) at energies of ~ 500 eV onto substrates plays a key role in reactive ion etching of SiO_2. However, the ion dynamics on the surface has not been fully clarified.

To date, many investigations on ion-surface interactions in a range of energies from meV to MeV have been reported. However, most of them deal with the molecular (polyatomic) ions H_2^+, D_2^+, D_3^+, N_2^+, O_2^+, and CO^+,[7–12] which are mainly dilution gases rather than the principal gases in plasma processings. We have recently reported ion scattering from metal surfaces bombarded with hydrocarbon ions (CH_x^+; $x=2$, 3, 4)[13] and fluorocarbon ions (CF_x^+; $x=1,2,3$).[14] In these experiments, aluminum instead of silicon compounds was chosen to eliminate chemical processes and to simplify the ion-surface interactions. Fluorocarbon ions were observed to dissociate into fragment ions at high impact energies (>100 eV), while the surface dissociation of hydrocarbon ions takes place at low energies (<50 eV) and high energies (>100 eV). As an extension of these previous works, we report here the measurement of ion survival rates and compare the surface dissociation of CH_x^+ ions with that of CF_x^+ ions.

II. ENERGY DISTRIBUTIONS OF SCATTERED IONS

The experiment was performed in an apparatus consisting of three differentially pumped regions: the plasma source region at 1 mTorr, the ion selection region at $\sim 10^{-5}$ Torr and the ion-surface interaction region $\sim 10^{-6}$ Torr. A detail of the apparatus was reported previously.[13,14] In the plasma source region, an inductively coupled discharge of 13.56 MHz, 40 W in CF_4 (or CH_4/Ar) yields a low-pressure fluorocarbon plasma (or methane plasma) of density $\sim 10^{10}$ cm^{-3} and potential $V_p = 15$–30 V. As shown in Fig. 1, many species of ions effusing from the plasma through an orifice are discriminated into a single species with a quadrupole mass filter in the ion selection region. The selected species of ion beam of 5 mm in diameter enters the ion-surface interaction region, and impinges on an aluminum target in a metal cage with an incident angle $\theta_i=45°$ with respect to the surface normal on the target plane. The incident ion energy E_i is given by $E_i=e(V_p-V_T)$ where V_T denotes the bias voltage of the target and the cage. As soon as the CH_x^+ or CF_x^+ beam is turned on, the target surface is covered with thin film layers of hydrocarbon or fluorocarbon, and hence, the top surface cannot be regarded as pure aluminum surface.

The ions scattered in the specular direction ($\theta_s=45°$) are measured with a quadrupole mass analyzer (QMA) which is biased at the voltage ΔV against the target and the cage. For example, Fig. 2(a) shows raw data of a spectrum of ions scattered from the target with which CF_3^+ ions collide at 100

[a]Electronic mail: sugai@nuee.nagoya-u.ac.jp

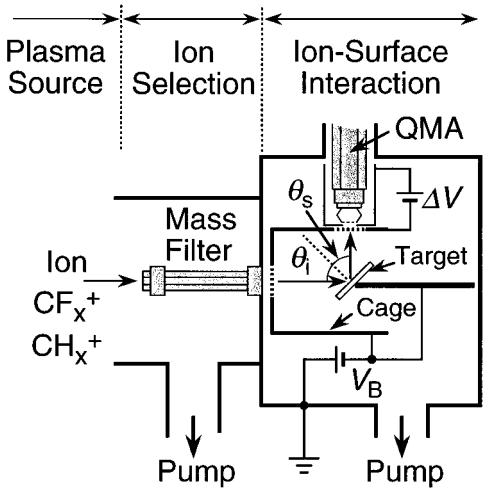

FIG. 1. Part of an experimental apparatus.

eV. The dissociated ions of CF^+ and CF_2^+ are observed in addition to the reflected ion CF_3^+. Figure 2(b) displays a series of dissociated ions (CH_2^+, CH^+, C^+, H^+) and the reflected ion CH_3^+ which are observed for the incidence of CH_3^+ ions at a very low energy of 20 eV.

As shown in Fig. 3(a), the energy spread of the ion beam impinging on the target was estimated to be a full width at half-maximum (FWHM) of ~18 eV from the derivative of ion current flowing to the grounded target with respect to the retarding bias V_T. Such a wide spread is probably caused by rf/dc voltages used in the quadrupole mass filter and was

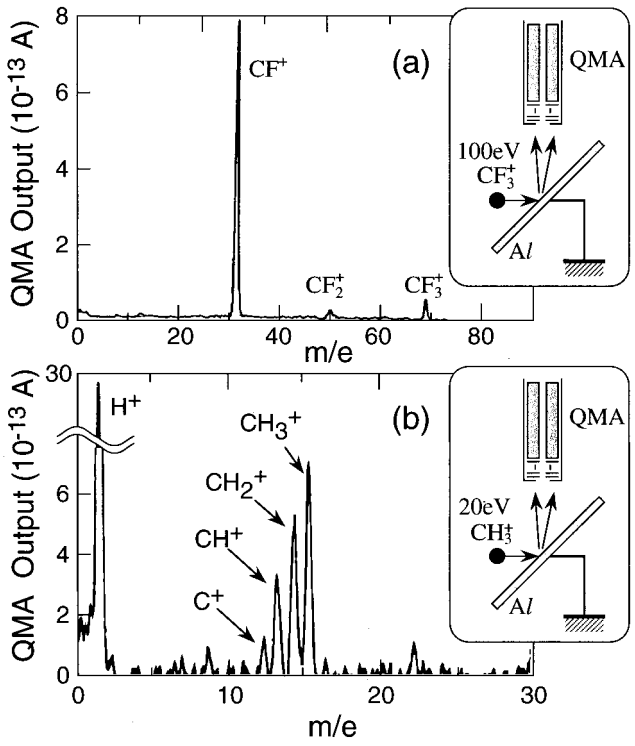

FIG. 2. Mass spectrum of ions scattered at 45° from an aluminum surface on which (a) 100 eV CF_3^+ ions and (b) 20 eV CH_3^+ ions are bombarded at 45°.

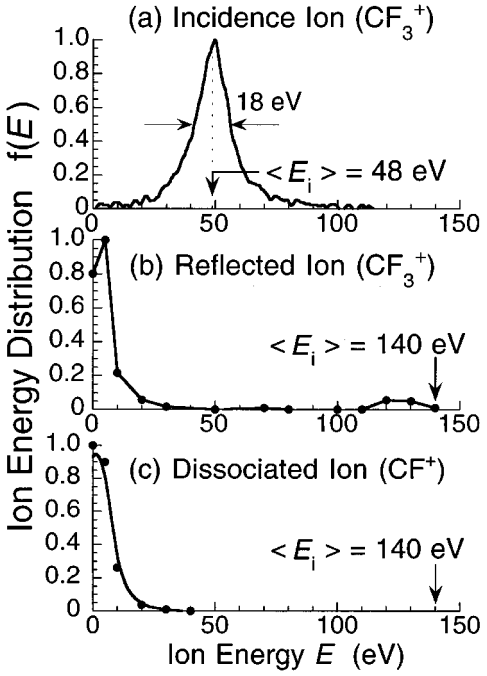

FIG. 3. Energy distributions of (a) incident ion CF_3^+ at $\langle E_i \rangle = 48$ eV, (b) reflected ion CF_3^+, and (c) dissociated ion CF^+ from the incidence of CF_3^+ at $\langle E_i \rangle = 140$ eV.

independent of the average incident energy $\langle E_i \rangle$. On the other hand, in order to obtain information on energies of scattered ions, the retarding voltage ΔV applied to the whole QMA region was positively increased to repel low-energy ions. Examples of the energy distribution functions obtained in this way are shown in Figs. 3(b) and 3(c) for the reflected ion CF_3^+ and the dissociated ion CF^+, respectively, in the case of the CF_3^+ incident at $\langle E_i \rangle = 140$ eV. As seen in Fig. 3(b), most of scattered ions have kinetic energies lower than 10 eV while a small fraction of the reflected ions has high energies comparable to the incident energy as recognized. We have discussed previously[14] how an elastic binary collision model qualitatively accounts for the low-energy part while the high-energy part may be understood taking account of recoil and cascade collisions.

III. ION SURVIVAL RATE

When positive ions XY^+ impinge on a metal target, most of them will be neutralized and are adsorbed on the surface or scattered as neutral species (XY, X, or Y). Only a trace of incident ions is backscattered as positive ions (XY^+, X^+, or Y^+) after collisions. Here we introduce the ion survival rate as a ratio of the total scattered ion flux to the incidence ion flux. This rate can be measured as a ratio of the cage current I_c to the target current I_T in the system shown in Fig. 4(a). The cage current often contains not only scattered ions but also secondary electrons ejected from the target. The effect of secondary electrons on I_c is clearly seen in Fig. 4(b), when the retarding voltage $(V_T - V_c)$ is varied for 150 eV CF_3^+ incidence. Here a grid is inserted and biased at $V_G = V_T$

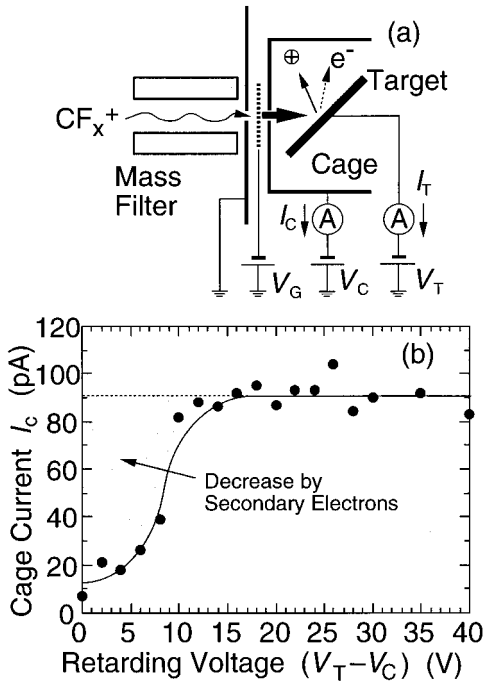

FIG. 4. (a) Experimental scheme for measurement of ion survival rate. (b) Cage current I_c vs retarding voltage $(V_T - V_c)$ for CF_3^+ incidence at 150 eV, where the shaded region indicates the current decrease due to secondary electron capture.

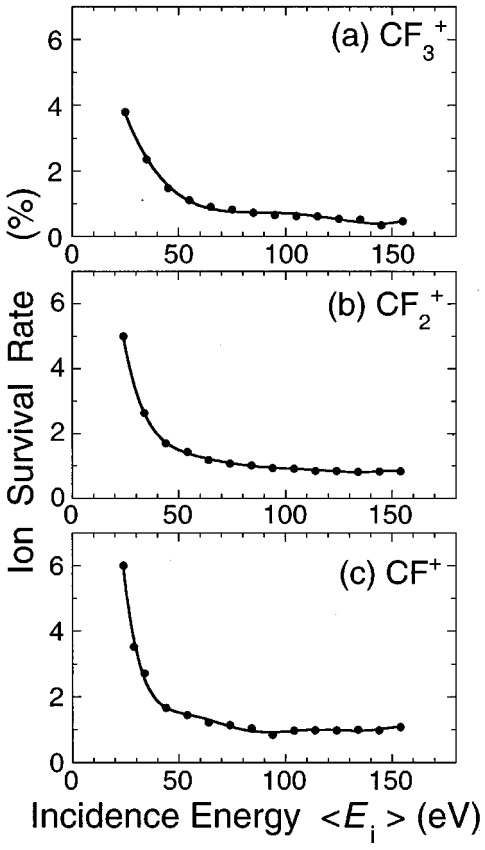

FIG. 5. Ion survival rate as a function of incident energy for (a) CF_3^+, (b) CF_2^+, and (c) CF^+ ion impinge at 45° on to an aluminum surface.

to minimize the field disturbance caused by a change in V_c. As a consequence, the bias V_c is lowered by ~ 15 V against the target voltage to suppress the secondary electrons whose kinetic energy is usually <15 eV.

In this way, the ion survival rates were measured as a function of incident energy and plotted for the fluorocarbon ions (CF_x^+, $x=1-3$) and hydrocarbon ions (CH_x^+, $x=2-4$) in Figs. 5 and 6, respectively. The survival rate of any incident ion species is relatively high at the energies lower than 50 eV while it is almost constant for the higher energies. The survival rates of hydrocarbon ions are smaller than the fluorocarbon ions by a factor of 2–3. Typical values of the survival rate are 0.3% for CH_x^+ ions and 1% for CF_x^+ ions. The composition of backscattered ions will be described in Sec. IV.

IV. DISSOCIATIVE ION BACKSCATTERING

As shown in Fig. 2, various ion species are backscattered from the target and, among them, our major interest is focused on the dissociated ions in view of dissociation physics and modification of radical composition in actual plasma reactors. Since the high-energy component is negligible (see Fig. 3), the total amount of scattered ions can be approximated from the QMA signal at the retarding bias $\Delta V=0$, i.e., the detection of ions of almost zero energy. In this way, the relative yields of scattered ion species were measured as a function of the incident energy in case of CF_x^+ incidence ($x=1-3$) and CH_x^+ ($x=2-4$) incidence, as reported previously.[13,14] Examples of CF_3^+ incidence and CH_4^+ incidence are shown in Fig. 7.

In order to obtain the branching ratio among the dissociated ion species, the vertical scale in Fig. 7 was calibrated as follows: First, the QMA outputs for each ion species are normalized by the target ion current to give the scattering yield per incident ion flux. Second, the mass discrimination effect of QMA is calibrated by comparing the CF_4 fragment patterns of the QMA with the known ionization cross sections of CF_4[15] and CH_4.[16] Finally, a change in the QMA sensitivity associated with the beam energy control (the bias V_B) is also checked. Thus, the scattered ion yields are commonly scaled in Fig. 7 and the measured yields can be compared among each other. However, the energy dependence was measured at the fixed angle $\theta_s=\theta_i=45°$, and hence, it is correct only if the angular distribution of scattered ions is independent of $\langle E_i \rangle$ and ion species.

Figure 7(b) (CH_4^+ incidence) suggests that there exist two types of dissociative back scattering depending on the incidence energies. One is the dissociation into relatively large molecular ions (CH_3^+, CH_2^+) at the low incidence energies (<50 eV). The other is the dissociation into small fragment ions (H^+, C^+, CH^+) at the high-energy incidence (>100 eV). The former is tentatively interpreted as a result of vibrational excitation induced by polyatomic-ion collision with

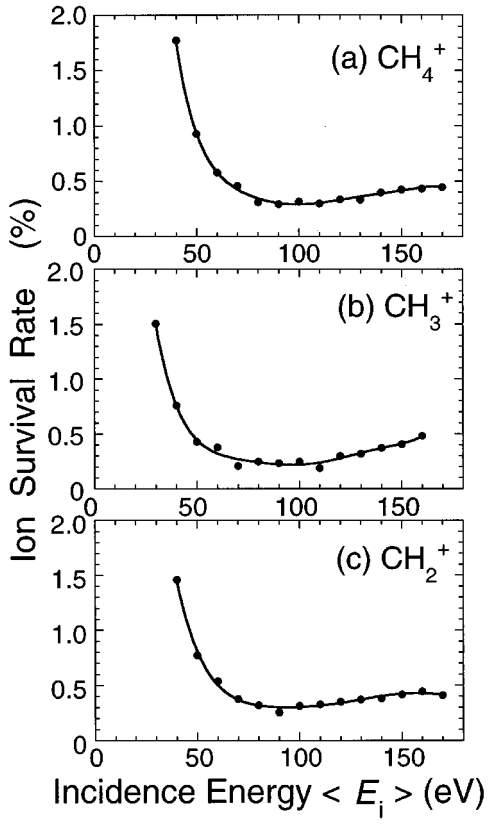

FIG. 6. Ion survival rate as a function of incident energy for (a) CH_4^+, (b) CH_3^+, and (c) CH_2^+ ion impinge at 45° onto an aluminum surface.

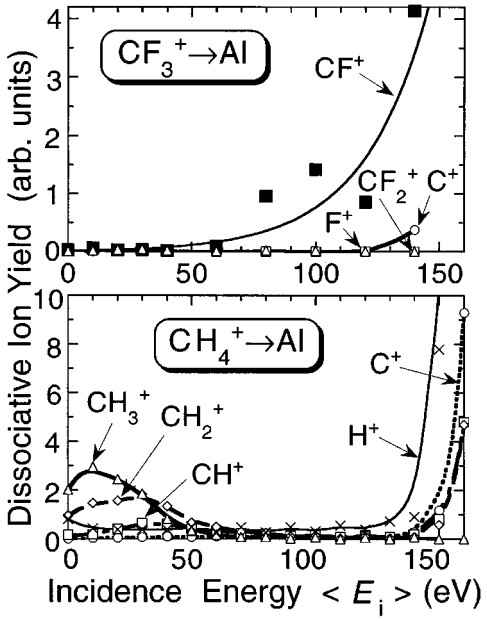

FIG. 7. Dissociative ion yield on the aluminum target bombarded with (a) CF_3^+ and (b) CH_4^+ beams as a function of the incidence energy $\langle E_i \rangle$. $\theta_i = \theta_s = 45°$ and $\Delta V = 0$.

solid surface while the latter is attributed to electronic excitations.[13,14]

The dissociative backscattering at high impact energies (>100 eV) is also observed in the case of fluorocarbon ions [see Fig. 7(b)]. In general, energetic ion bombardment may sputter the already deposited fluorocarbon layers, producing various fluorocarbon ions. In fact, we observed CF_x^+ signals when the target is bombarded with argon ions at similar high energies and fluxes. However, the signals were more than one order of magnitude smaller compared with the case of fluorocarbon ion bombardment. If sputtering were dominant, the impact of the CF_x^+ beam would yield not only smaller ion species but larger species such as CF_{x+1}^+ ($x=1-2$). However, only smaller fragments were observed in the present experiment. Thus, the sputtering process is not a major source of the observed ion scattering at high energies.

When Fig. 7(a) is compared with Fig. 7(b), one notices a remarkable difference in a range of incidence energy lower than 50 eV: fluorocarbon ions hardly break up into smaller fragment ions on the surface at such low impact energies in contrast to the hydrocarbon ions. This difference may come from a large difference in the bond dissociation energies: $\Delta E = 5.4$ eV for $CF_3^+ \rightarrow CF_2^+ + F$ and $\Delta E = 0.67$ eV for $CH_4^+ \rightarrow CH_3^+ + H$. Thus, the CF_3^+ ion has a deep well in the potential curve of the electronic ground state, so that vibrational excitation induced by low-impact energies cannot give rise to dissociation.

ACKNOWLEDGMENTS

The authors would like to thank Toshiba Corporation for its technical and financial support. This work was supported by a Grant-in-Aid for Scientific Research from the Ministry of Education, Science, Sports and Culture in Japan.

[1]For a review, see J. C. Angus, P. Koidl, and S. Domitz, in *Plasma Deposited Thin Films*, edited by J. Mort and F. Jansen (CRC, Boca Raton, FL, 1986), p. 89.
[2]H. Sugai, H. Kato, and T. Okubo, Nucl. Instrum. Methods Phys. Res. B **23**, 552 (1987).
[3]J. Wagner, Ch. Wild, F. Pohl, and P. Koidl, Appl. Phys. Lett. **48**, 106 (1989).
[4]Y. Yamashita, H. Toyoda, and H. Sugai, Jpn. J. Appl. Phys., Part 2 **28**, L1647 (1989).
[5]Y. Yamashita, K. Katayose, H. Toyoda, and H. Sugai, J. Appl. Phys. **68**, 3735 (1990).
[6]K. Katayose, H. Toyoda, and H. Sugai, Kaku-Yugo Kenkyu **67**, 51 (1992).
[7]W. Eckstein, H. Verbeek, and S. Datz, Appl. Phys. Lett. **27**, 527 (1975).
[8]B. Willerding, W. Heiland, and K. J. Snowdon, Phys. Rev. Lett. **53**, 2031 (1984).
[9]P. Haochang, T. C. Horn, and A. W. Kleyn, Phys. Rev. Lett. **57**, 3035 (1986).
[10]H. Akazawa and Y. Murata, Surf. Sci. **207**, L971 (1989).
[11]H. Akazawa and Y. Murata, J. Chem. Phys. **92**, 5551 (1990).
[12]H. Akazawa and Y. Murata, J. Chem. Phys. **92**, 5560 (1990).
[13]Y. Mitsuoka, H. Toyoda, and H. Sugai, Jpn. J. Appl. Phys., Part 2 **34**, L516 (1995).
[14]Y. Mitsuoka, H. Toyoda, and H. Sugai, Jpn. J. Appl. Phys., Part 2 **34**, L1486 (1995).
[15]C. Ma, M. R. Bruce, and R. A. Bonham, Phys. Rev. A **44**, 2921 (1991).
[16]H. Chatham, D. Hils, R. Robertson, and A. Gallagher, J. Chem. Phys. **81**, 1770 (1984).